

## CBETA: First Multipass Superconducting Linear Accelerator with Energy Recovery

A. Bartnik, N. Banerjee<sup>1</sup>, D. Burke, J. Crittenden<sup>1</sup>, K. Deitrick<sup>1</sup>, J. Dobbins<sup>1</sup>, C. Gulliford<sup>1</sup>,  
G. H. Hoffstaetter<sup>1</sup>, Y. Li, W. Lou, P. Quigley, D. Sagan<sup>1</sup>, and K. Smolenski<sup>1</sup>

*Cornell Laboratory for Accelerator Based Sciences and Education, Cornell University, Ithaca, New York 14850, USA*

J. S. Berg, S. Brooks<sup>2</sup>, R. Hulsart, G. Mahler, F. Meot, R. Michnoff, S. Peggs, T. Roser<sup>2</sup>,  
D. Trbojevic<sup>2</sup>, and N. Tsoupas<sup>2</sup>

*Brookhaven National Laboratory, Upton, New York 11973-5000, USA*

T. Miyajima

*High Energy Accelerator Research Organization (KEK), Oho, Tsukuba, Ibaraki 305-0801, Japan*



(Received 5 May 2020; accepted 9 June 2020; published 23 July 2020)

Energy recovery has been achieved in a multipass linear accelerator, demonstrating a technology for more compact particle accelerators operating at higher currents and reduced energy consumption. Energy delivered to the beam during the first four passes through the accelerating structure was recovered during four subsequent decelerating passes. High-energy efficiency was achieved by the use of superconducting accelerating cavities and permanent magnets. The fixed-field alternating-gradient optical system used for the return loop successfully transported electron bunches of 42, 78, 114, and 150 MeV in a common vacuum chamber. This new kind of accelerator, an eight-pass energy recovery linac, has the potential to accelerate much higher current than existing linear accelerators while maintaining small beam dimensions and consuming much less energy per electron.

DOI: [10.1103/PhysRevLett.125.044803](https://doi.org/10.1103/PhysRevLett.125.044803)

*Introduction.*—The Cornell-BNL ERL Test Accelerator (CBETA) [1] is a multiturn energy recovery linac (ERL) that has successfully demonstrated four acceleration and four deceleration passes through its superconducting linac, constructed and commissioned at Cornell University as a collaborative effort with Brookhaven National Laboratory. It simultaneously transports electron beams with four energies ranging from 42 to 150 MeV in a single fixed-field alternating-gradient (FFA) beam line. The FFA beam line uses permanent magnets, thus requiring no electrical power to operate.

Potential applications of these technologies include medical isotope production, cancer therapy, x-ray sources, and industrial applications such as microchip production, as well as more energy-efficient machines for basic research in physics, materials science, and many other fields. In particular, only ERL technology currently seems capable of producing the beam power required to efficiently cool ions at the Electron-Ion Collider (EIC), a groundbreaking nuclear physics research facility to be constructed at Brookhaven National Laboratory. The CBETA project allows the study and measurement of many critical phenomena relevant to both the EIC and ERL communities, including the beam-breakup instability [2], halo development and collimation, as well as growth in energy spread by coherent synchrotron radiation (CSR) and microbunching.

An ERL uses the same radio-frequency (rf) cavities to accelerate and then decelerate the recirculated beam, recovering the beam energy into the electromagnetic fields of the cavities. When superconducting rf (SRF) cavities are used, the energy is stored nearly loss free and the energy can then be used to accelerate subsequent particles, thus requiring low input power to create a very high power beam. ERLs were first proposed in 1965 [3] and first demonstrated in 1987 [4]. Several ERLs with one acceleration pass have been operated. Among them, Jefferson Lab has achieved the highest continuous beam power with an electron beam of about 10 mA accelerated to about 100 MeV [5,6]. S-DALINAC in Darmstadt [7] and cERL at KEK [8] are currently in operation. Novosibirsk has built and operated an ERL with four accelerating and four decelerating passes [9], but their room-temperature rf cavities cannot store energy for long enough to use it to accelerate new beams, instead only providing an efficient way to absorb the beam energy. Achieving high-efficiency ERL operation requires SRF cavities.

CBETA is the first SRF ERL with multiple acceleration and deceleration passes. A multipass ERL allows one to achieve the high efficiency of an ERL with a much smaller linac and therefore a significant reduction in cost and size. One can construct separate beam lines for each energy to transport the beam to the linac, as was done at Novosibirsk [9]. Instead, CBETA has a single FFA return loop for all

TABLE I. CBETA machine parameters.

Parameter	Value	Units
Bunch charge, design limit	125	pC
Bunch charge, commissioning	5	pC
Bunch rate, design limit	325	MHz
Bunch rate, commissioning	< 1	kHz
Beam current, design limit	40	mA
Beam current, commissioning	1	nA
Beam energy, injector	6	MeV
Beam energy, peak	150	MeV

four returned beam energies, saving construction and operating costs.

The FFA optical design transports a wide range of beam energies in a single beam line without the need to vary the magnetic fields. FFAs were first proposed and built in the 1950s [10–12], but were supplanted by other accelerator technologies, until a revival in Japan in the 1980s, when a series of machines were constructed [13,14]. The basis of the original “scaling” designs was to keep the particle oscillation frequencies unchanged with beam energy. Nonscaling FFA designs were proposed [15,16] that allowed this frequency to vary. In principle this causes problems with resonances, but this difficulty can be overcome by using linear focusing magnets [16]. Such a linear nonscaling FFA (FFA LG) ring was built at Daresbury (EMMA) [17], and demonstrated transport of a beam over a factor of 1.7 in beam energy. A shorter beam line [18] demonstrated transport with a much larger factor in energy. CBETA’s return line uses such FFA LG optics to transport any beam energy between 42 and 150 MeV.

The return loop combines other novel technologies, such as the use of Halbach combined-function permanent magnets [19,20] and an adiabatic transition between the arc and straight sections [21]. We present here results demonstrating recovery of the beam energy in the linac and transport of multiple beam energies in the FFA return loop.

Table I shows both the design and commissioning parameters for CBETA. The commissioning period reported here established multiturn energy recovery at low currents of about 1 nA. A conservative, safe current level was used for equipment and personnel protection, to avoid radiation damage to the permanent magnets and to have an acceptable radiation level in areas adjacent to the accelerator. A reduced bunch charge of 5 pC was also used to avoid particle loss from CSR. A push to high current will be the next stage of this accelerator. This Letter will discuss the first multipass operation with energy recovery to date.

The layout of the CBETA accelerator is shown in Fig. 1. The Cornell injector [22–24] begins with a dc photoelectron gun operated at 300 kV, a pair of emittance compensating solenoids, and a normal-conducting buncher cavity. This is immediately followed by the injector cryomodule (ICM), accelerating the beam to the target

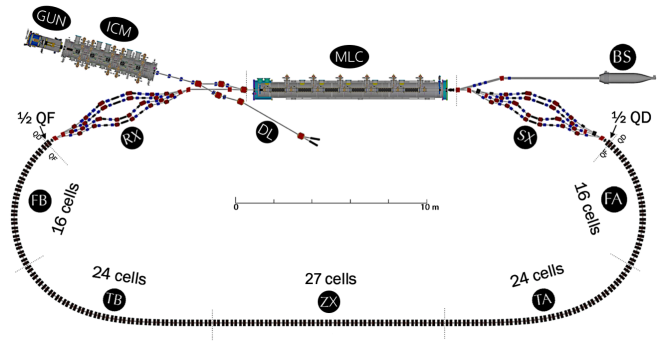


FIG. 1. The major components of CBETA are the electron gun (GUN), the injector cryomodule (ICM), the main linac cryomodule (MLC), the diagnostic line (DL), the four splitter-combiner lines (SX), the FFA arc consisting of the first arc (FA), first transition (TA), straight section (ZX), second transition (TB), second arc (FB), and the four splitter-combiner lines (RX). The fully decelerated beam is absorbed in the beam stop (BS).

injection energy of 6 MeV. The beam is then steered either left through a three-bend achromatic merger into the main linac cryomodule (MLC) cavities or into a set of transverse and longitudinal diagnostics. The layout of the mirror merger and the position of the diagnostics are chosen such that the bunch can be studied in a location equivalent to the beginning of the first MLC cavity, downstream of which the effects of space charge are greatly reduced. The MLC itself consists of six cavities, providing a total energy gain of 36 MeV. The energy gain and phase of each cavity are not equal, and instead are chosen to account for non-relativistic effects [25] and to minimize the growth of the energy spread throughout the machine.

The higher-energy beams downstream of the MLC are guided into the four SX “splitter” beam lines by a common electromagnet. These beam lines serve to match independently the optics of each beam required at the entrance of the return loop. Each of the four beam lines contains 8 quadrupole magnets, up to 10 dipole magnets, and a motorized path length adjusting chicane. The number of quadrupoles was chosen to allow enough flexibility to match the beam optics functions into the single FFA return arc, while the dipoles and chicane allow tuning of the FFA injection orbit and arrival time.

The FFA return loop is strongly focusing; it consists of Halbach style permanent magnets [26] of two types, a focusing quadrupole and a defocusing gradient dipole [27,28]. The first and last magnets in the loop are half-length magnets which aid the transitions to and from the splitters. The rest of the FFA magnets are arranged in focusing and defocusing pairs in a periodic doublet configuration. The FFA lattice design was verified using independent accelerator physics codes [29–31]. Each permanent magnet has either a vertical or horizontal dipole corrector, which is used to correct misalignments or small field errors in the permanent magnets. The maximum field

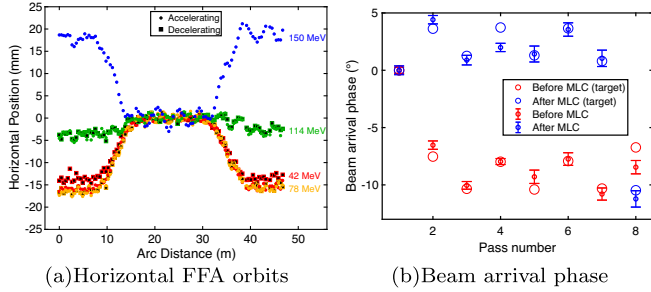


FIG. 2. Measured orbits through the FFA and arrival time before and after the MLC. Arrival time is shown in units of rf phase, and the phases of the decelerating passes are shown relative to  $180^\circ$ .

in the dipole correctors is equivalent to the field produced by a magnet misalignment of 3 mm.

The FFA return loop consists of three types of sections: arc, straight, and the transitions between them. In the arc sections, the beam trajectories for the four energies are spatially separated, with the highest energy on the outside of the arc. In the transition sections, the four orbits converge adiabatically toward the center of the pipe, and the periodic optics functions change adiabatically into those of the straight section [21].

Downstream of the FFA, the four beams are separated into the RX splitter lines. Their trajectory, optics functions, and path lengths again are individually tuned for further passes through the MLC. Finally, the energy-recovered 6 MeV beam is guided to the beam stop.

*Results.*—Figure 2(a) shows the measured beam orbits through the common FFA loop, demonstrating that the design trajectories were achieved. Because beam position monitors (BPMs) are placed in periodic positions in the FFA loop, the design orbit maintains periodic values in the arc and straight sections, with adiabatic transitions between them. The beam arrival phases at the entrance and exit of the MLC are shown in Fig. 2(b) and compared to the target values from simulation. All phases are shown with respect to their values from the first pass through the MLC, with the sign chosen such that negative phases indicate a later arrival time. Compared to the first pass, higher passes show a systematically later arrival at the BPM before the MLC because the first-pass beam is the slower beam from the injector. On top of that systematic offset, each pass is intentionally alternated slightly positive or negative to prevent growth in energy spread while maintaining energy balance.

Figure 3 compares the measured and designed betatron tunes as a function of the beam energy, showing that the orbits, rf phases, and optics functions are close to their design values. Tunes were measured by kicking the beam either horizontally or vertically in the splitter line before each pass, and fitting a sine function to the resulting orbit difference. In addition to the four design energies, we also

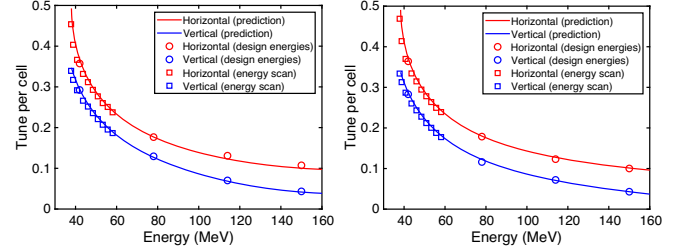


FIG. 3. Measured tunes in the FFA arc sections (left) and straight section (right) as a function of beam energy. The lines show the result of a field map-based model calculation.

performed a scan of the first-pass energy from 39 to 60 MeV by varying the energy gain in the MLC. Tunes show good agreement with simulated predictions from fieldmap-based particle tracking.

While trajectories, rf phases, and optics propagation in the FFA are close to the design, and while each particle arriving at the beam stop has had its energy recovered, not all particles made it through all eight passes. Figure 4(a) shows an image of the remaining beam on the view screen at the entrance to the beam stop, and Fig. 4(b) shows a measure of the transmission throughout the machine. We were able to recover the energy of about one third of the beam, the rest being lost after the sixth pass. The data suggest a slow loss of transmission, beginning as early as the second pass, accumulating up to around 10% total loss by the end of the sixth pass through the FFA, followed by a much larger drop in transmission before entering the seventh pass. Investigations into the source of these losses uncovered many small problems in optics settings, non-linear stray fields, evidence of microbunching, and others, but these have not yet been fully investigated. It was clear, however, that additional diagnostics for the energy recovery passes are needed to solve this problem—either partially interceptive screens similar to those at Darmstadt [32] or other noninterceptive diagnostics.

*Commissioning procedures.*—Commissioning of CBETA naturally splits into two separate efforts. In the low-energy

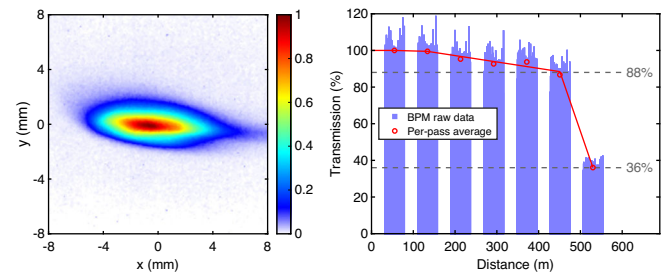


FIG. 4. Left: Image of the beam on the view screen before beam stop. Right: Transmission for each of the seven passes through the FFA arc. Blue bars are a scaled reading of charge from individual BPMs, red circles are an average of that data over each pass. Red lines are included as a guide to the eyes.

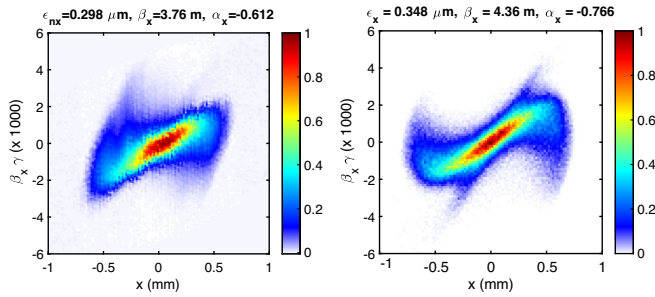


FIG. 5. Measured (left) and simulated (right) transverse phase spaces after the injector at 5 pC.

injector, space-charge effects dominate, and obtaining the best beam quality relies on compensating their emittance-diluting effects. The primary diagnostic is thus the emittance measurement system (EMS) in the diagnostic line (DL). Space-charge effects are relatively minor following the first-pass acceleration through the MLC. Commissioning efforts then switch to achieving the desired orbit, energy, and dispersion through the rest of the machine.

For characterization of the injector beam, the beam is diverted into the DL composed of a suite of diagnostics, including the EMS [33,34], a vertical deflecting cavity [35], and an energy spectrometer (dipole magnet) for measuring the longitudinal phase space of the beam. The placement of the EMS at a position corresponding approximately to that of the first MLC cavity allows for detailed characterization of the beam entering the MLC.

To determine suitable machine settings for the low-energy injector, a multiobjective genetic algorithm optimization [22–24] is applied to 3D space-charge simulations of the beam passing through injector, merger, and MLC. These optimal settings are then loaded into the injector and small magnet adjustments made to produce the correct phase space ellipse.

Figure 5 shows an example of the measured horizontal phase space near a representative optimized injector setting determined from simulations, as well as the corresponding results of simulations at the operating setting.

Orbit correction methods differed in each section of the machine. In the MLC, the beams were centered in the rf cavities; in the splitter sections, the beam was centered in the quadrupoles. Particularly in the FFA return loop, with its seven beams of four energies, orbit correction is unconventional, since the corrector coils act on all beams. In general, orbit correction used a singular-value decomposition algorithm where the rms orbit deviation of all beams are minimized using either a predicted or measured response matrix. Predicted responses were effective only for single beams over short distances, with measured responses required for more complex corrections. As an example, the orbits in the FFA are shown before and after simultaneously correcting the first three passes in Fig. 6.

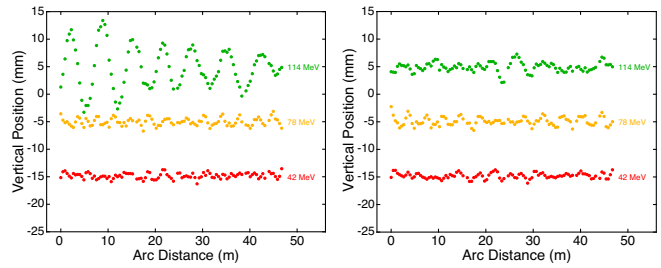


FIG. 6. Measured vertical orbits of the first three passes through the FFA return loop before (left) and after (right) application of a simultaneous orbit correction algorithm. Orbits are offset for clarity.

The splitters are designed to match optics functions and orbits at the entrances and exits of the FFA return loop and the MLC, and to adjust overall path length of the arc for arrival time at the MLC. BPMs were used to directly measure the orbit and path length, and the correction of these quantities was straightforward. In order to correct the beam optics functions, we begin with a machine setting from simulation, and then tune from there. In practice, we are limited to a direct measurement of the dispersion functions and the transport matrix element  $R_{56}$ , which describes the energy dependence of the beam’s position and arrival time, and our optics correction focuses on those. Correction in a given splitter line was done by measuring the response to each splitter quadrupole, which could then be used to predict corrections. Throughout this correction, changes to the beam size were ignored, and thus corrections to dispersion and  $R_{56}$  were iterated with manual corrections to maintain beam size. These procedures were used only on the first four passes through the machine, when there are single beams in the splitter lines. For the decelerating passes, a manual, empirical tuning approach was used to maximize transmission into the beam stop, iteratively making small adjustments to all magnet settings while monitoring only the final transmission.

The next step is to improve transmission, which includes investigating better optics solutions, developing improved diagnostics for the decelerating passes, and reducing halo by using a low halo cathode possibly in conjunction with collimation.

*Summary.*—The first multiturn superconducting energy recovery linac has operated in energy-recovery mode. The construction and commissioning team developed procedures specific to this new type of accelerator. The beam spot following eight-pass energy recovery was measured, the seven beam orbits in the common FFA return arc were measured and corrected, and the beam flight time and matching optics functions were successfully tuned. This Letter provides proof of principle for the most energy-efficient technologies to be applied in the design and operation of future high-performance particle accelerators.

This work was supported by NSF Grant No. DMR-0807731, DOE Award No. DE-SC0012704, and NYSERDA Agreement No. 102192.

- 
- [1] G. H. Hoffstaetter, D. Trbojevic *et al.*, CBETA Design Report, Cornell-BNL ERL Test Accelerator, Technical Report, [arXiv:1706.04245](https://arxiv.org/abs/1706.04245).
- [2] W. Lou and G. H. Hoffstaetter, *Phys. Rev. Accel. Beams* **22**, 112801 (2019).
- [3] M. Tigner, *Nuovo Cimento* **37**, 1228 (1965).
- [4] T. Smith, H. Schwettman, R. Rohatgi, Y. Lapiere, and J. Edighoffer, *Nucl. Instrum. Methods Phys. Res., Sect. A* **259**, 1 (1987).
- [5] G. R. Neil *et al.*, *Nucl. Instrum. Methods Phys. Res., Sect. A* **557**, 9 (2006).
- [6] G. R. Neil *et al.*, *Phys. Rev. Lett.* **84**, 662 (2000).
- [7] M. Steinhorst, M. Arnold, and N. Pietralla, in *Proceedings of the 27th Linear Accelerator Conference (LINAC2018), Beijing, 2018* (JACoW Publishing, Geneva, 2018), pp. 706–709.
- [8] T. Obina *et al.*, in *10th International Particle Accelerator Conference* (2019), pp. TUPGW036, <http://accelconf.web.cern.ch/ipac2019/papers/tupgw036.pdf>.
- [9] O. A. Shevchenko *et al.*, in *Proceedings of the 37th International Free Electron Laser Conference*, edited by H. S. Kang, D.-E. Kim, and V. R. Schaa (JACoW, Daejeon, Korea, 2015), pp. 1–4.
- [10] F. R. Symon, D. W. Kerst, L. W. Jones, L. J. Laslett, and K. M. Terwillger, *Phys. Rev.* **103**, 1837 (1956).
- [11] T. Ohkawa, in *Proceedings of the Symposium on Nuclear Physics of the Physical Society* (1953).
- [12] A. A. Kolomenskii, *Zh. Eksp. Teor. Fiz.* **33**, 298 (1957) [*Sov. Phys. JETP* **6**, 231 (1957)].
- [13] M. Yoshimoto, T. Adachi, M. Aiba, S. Machida, Y. Mori, A. Muto, R. Muramatsu, C. Ohmori, I. Sakai, Y. Sato, M. Sugaya, A. Takagi, R. Ueno, A. Yamazaki, T. Yokoi, U. Yonemura, M. Yoshii, Y. Yuasa, and K. Koba, in *Proceedings of the 8th European Accelerator Conference (EPAC 2002), Paris, 2002* (JACoW Publishing, Paris, France, 2002), pp. 1320–1322.
- [14] S. Machida, Y. Mori, A. Muto, J. Nakano, C. Otori, I. Sakai, Y. Sato, A. Takagi, T. Y. M. Yoshii, M. Yoshimoto, Y. Yuasa, M. Matoba, Y. Yonemura, A. Yamazaki, T. Uesugi, M. Aiba, and M. Sugaya, in *Proceedings of the 9th European Accelerator Conference (EPAC 2004), Lucerne, Switzerland, 2004* (JACoW Publishing, Lucerne, Switzerland, 2004), pp. 2643–2645.
- [15] D. Trbojevic, E. D. Courant, and A. Garren, *AIP Conf. Proc.* **530**, 333 (2000).
- [16] C. Johnstone, W. Wan, and A. Garren, *Conf. Proc. C* **990329**, 3068 (1999).
- [17] S. Machida *et al.*, *Nat. Phys.* **8**, 243 (2012).
- [18] Brookhaven National Laboratory, News Report- Media & Communications Office, 1, 2017, <https://www.bnl.gov/newsroom/news.php?a=212405>.
- [19] S. Brooks, J. Cintorino, A. Jain, and G. Mahler, in *Proceedings of the 8th International Particle Accelerator Conference* (2017), p. THPIK007.
- [20] S. Brooks, G. Mahler, R. Michnoff, and J. Tuozzolo, in *Proceedings of the 10th International Particle Accelerator Conference* (2019), p. THPTS088.
- [21] J. S. Berg, S. Brooks, F. Méot, D. Trbojevic, N. Tsoupas, J. Crittenden, Y. Li, and C. Mayes, in *Proceedings of the 59th ICFA Advanced Beam Dynamics Workshop on Energy Recovery Linacs (ERL2017)*, Geneva, Switzerland, edited by M. Draper and S. Ramberger (JACoW, Geneva, Switzerland, 2018), pp. 52–57.
- [22] C. Gulliford, A. Bartnik, I. Bazarov, L. Cultrera, J. Dobbins, B. Dunham, F. Gonzalez, S. Karkare, H. Lee, H. Li, Y. Li, X. Liu, J. Maxson, C. Nguyen, K. Smolenski, and Z. Zhao, *Phys. Rev. ST Accel. Beams* **16**, 073401 (2013).
- [23] C. Gulliford, A. Bartnik, I. Bazarov, B. Dunham, and L. Cultrera, *Appl. Phys. Lett.* **106**, 094101 (2015).
- [24] A. Bartnik, C. Gulliford, I. Bazarov, L. Cultrera, and B. Dunham, *Phys. Rev. ST Accel. Beams* **18**, 083401 (2015).
- [25] R. Koscica, N. Banerjee, G. H. Hoffstaetter, W. Lou, and G. Premawardhana, *Phys. Rev. Accel. Beams* **22**, 091602 (2019).
- [26] K. Halbach, *Nucl. Instrum. Methods* **169**, 1 (1980).
- [27] S. Brooks, Magnet and lattice specifications for the CBETA first girder, Technical Report No. CBETA-001, Brookhaven National Lab, 2016, [https://www.classe.cornell.edu/CBETA\\_PM/notes/CBETA001.pdf](https://www.classe.cornell.edu/CBETA_PM/notes/CBETA001.pdf).
- [28] W. Lou, A. Bartnik, J. S. Berg, S. Brooks, J. A. Crittenden, C. Gulliford, G. H. Hoffstaetter, F. Meot, D. Sagan, D. Trbojevic, and N. Tsoupas, in *Proceedings of the 9th International Particle Accelerator Conference (IPAC'18)*, Vancouver, Canada, 2018 (JACoW Publishing, Geneva, 2018), pp. 3000–3003.
- [29] F. Méot, N. Tsoupas, S. Brooks, and D. Trbojevic, *Nucl. Instrum. Methods Phys. Res., Sect. A* **896**, 60 (2018).
- [30] Opera 3D, Dassault Systems, 2019.
- [31] D. Sagan, *Nucl. Instrum. Methods Phys. Res., Sect. A* **558**, 356 (2006).
- [32] M. Arnold, J. Birkhan, J. Pforr, N. Pietralla, F. Schließmann, M. Steinhorst, and F. Hug, *Phys. Rev. Accel. Beams* **23**, 020101 (2020).
- [33] I. V. Bazarov, B. M. Dunham, C. Gulliford, Y. Li, X. Liu, C. K. Sinclair, K. Soong, and F. Hannon, *Phys. Rev. ST Accel. Beams* **11**, 100703 (2008).
- [34] H. Li, Mutli-dimensional characterization of the laser and electron beams of the Cornell energy recovery linac photoinjector prototype, Ph.D. Thesis, Cornell University, 2012.
- [35] S. Belomestnykh, I. Bazarov, V. Shemelin, J. Sikora, K. Smolenski, and V. Veshcherevich, *Nucl. Instrum. Methods Phys. Res., Sect. A* **614**, 179 (2010).